Influence of Artificial Periodicity and Ionic Strength in Molecular Dynamics Simulations of Charged Biomolecules Employing Lattice-Sum Methods

Mika A. Kastenholz and Philippe H. Hünenberger*

Laboratorium für Physikalische Chemie, ETH Zürich, CH-8093 Zürich, Switzerland

Received: April 23, 2003; In Final Form: November 3, 2003

Lattice-sum methods are nowadays routinely used to calculate electrostatic interactions in explicit-solvent simulations of biomolecular systems. These methods account for the long-range component of Coulomb interactions by assuming that they are exactly periodic within the simulated system. When lattice-sum methods are applied to inherently nonperiodic systems such as solutions, it is legitimate to question the validity of this assumption. The present study investigates the nature and magnitude of periodicity-induced artifacts in a set of 12 independent explicit-solvent molecular dynamics simulations of a small protein and an oligonucleotide, at different temperatures and ionic concentrations. Configurations sampled during these simulations are analyzed using continuum electrostatics to evaluate the corresponding periodicity-induced perturbation of the electrostatic free energy. The results suggest that, for the systems considered, artificial periodicity induces a nonnegligible free-energy bias in the sampled ensembles, but that this energetical bias results in no major structural perturbation. The perturbation is also found to be smallest when a minimal (neutralizing) set of counterions is included during the simulation.

Introduction

The recognition of the problem inherent to the evaluation of electrostatic potentials in condensed-phase systems under periodic boundary conditions (PBC) dates back to the classical article of Madelung.[1] Nowadays, lattice-sum methods[2−13] such as the Ewald,[2] particle−particle−particle−mesh (P^3M),[3] and (smooth) particle−mesh Ewald (PME or SPME)[4,5] methods are routinely used for computing electrostatic interactions in computer simulations of solvated (bio)molecules under PBC. Although originally developed to study ionic crystals,[1,2] the success of lattice-sum methods in the area of protein[14−16] and nucleic acid[15,17−19] simulations has led to a widespread use of these algorithms. As opposed to the traditional cutoff-truncation schemes,[20] lattice-sum methods permit the exact calculation of the Coulomb potential under PBC. The word "exact", however, should be used with some caution. Although rigorously enforcing periodicity is probably a reasonable approximation when crystals are simulated, it may not be so when considering inherently nonperiodic systems such as solutions. On one hand, including explicitly some description of the long-range component of electrostatic interactions is certainly to be favored. On the other hand, lattice-sum algorithms impose the artificial constraint of PBC to this long-range component, so that their application may lead to periodicity-induced artifacts. These need to be investigated thoroughly. In particular, artificial periodicity has been suspected to result in an overstabilization of the native structure of biomolecules and an inhibition of their conformational fluctuations.[21−25] From this point of view, the major alternative for the inclusion of a long-range electrostatic component in molecular simulations, i.e., the reaction-field method,[26−30] should not necessarily be viewed as less exact for simulating solutions. Rather, it results from a different approximation, namely, that the medium beyond the cutoff sphere of each particle behaves as a dielectric continuum of permittivity equal to that of the solvent. It appears that the use of the reaction-field method in molecular dynamics simulations also permits the generation of stable protein[31,32] and nucleic acid[33] trajectories.

The consequences of using lattice-sum methods to simulate liquids (and in particular water) have been previously investigated in the literature. Early studies have focused on the influence of boundary conditions on the calculation of the dielectric permittivity of pure liquids.[27,34−43] In terms of finite-size effects,[44−46] it was found that the distance-dependent Kirkwood g factor (which describes the average interaction of a water dipole with its coordination shells[47]) for water showed a significant rise beyond its value at the third coordination shell when lattice-sum methods were used with tinfoil boundary conditions. This indicates the presence of additional long-range correlations (i.e., the alignment of dipoles at large distances is artificially stabilized). The authors claim that the origin of the artifact lies in the use of tinfoil boundary conditions[6,7,27,48,49] rather than in the imposed periodicity. Similar problems with the application of tinfoil boundary conditions in the study of polar fluids have also been reported by other authors.[50,51] In contrast, it has also been argued that tinfoil boundary conditions are particularly well suited for simulating liquids and solutions when small box sizes are used, due to the elimination of the surface term.[52] However, even advocates for vacuum boundary conditions can be found,[53] with the argument that these boundary conditions reproduce better the results of finite-system simulations. Before the computational power allows for system sizes sufficiently close to the thermodynamic limit, the choice of the correct surface term is likely to remain an ongoing debate.

The artifacts that arise from the use of lattice-sum methods to compute free energies of ionic solvation are now well understood,[48,49,54−62] and appear to be of two kinds. The first kind of artifact is a negative free-energy (and pressure[61]) shift related to the Wigner self-energy[8,55,63−65] of a charge in a

* To whom correspondence should be addressed. Phone: +41-1-632-5503. Fax: +41-1-632-1039. E-mail: phil@igc.phys.chem.ethz.ch.

10.1021/jp0350924 CCC: $27.50
Published on Web 12/17/2003

periodic system (i.e., the interaction of the charge with its own periodic copies and a homogeneous neutralizing background charge density filling the infinite periodic system). For a spherical ion in a cubic unit cell, this free-energy shift can be calculated analytically on the basis of continuum electrostatics,[60] and depends on the ionic charge and radius, on the edge of the unit cell, and on the solvent permittivity. The second kind of artifact[53,58,66−70] is a second free-energy shift that arises because the average potential is zero in a system under PBC,[8,58] rather than the potential at infinity. In other words, the potential generated by the solvent at the ion site follows from a charge-based summation (q sum)[58,66,67,69] rather than from the (presumably) correct molecule-based summation (M sum),[53] resulting in a constant offset. For a spherical solvent molecule (single van der Waals interaction site), the corresponding free-energy shift can be calculated analytically,[53,66] and depends on the ionic charge, on the solvent density, and on the geometry of the charge distribution within the solvent molecule. Note that this second free-energy artifact is linear, while the first artifact is quadratic in the ionic charge.

Artifacts linked with the use of lattice-sum methods to study potentials of mean force (PMFs) for the interaction between two ions have also been discussed previously.[48,60,62,71−73] Clearly, an ion−ion PMF cannot possess the correct long-range behavior under PBC because of periodicity. In particular, two ions situated along a line parallel to an edge of the unit cell and separated by half the length of this edge cannot exert a mean force on each other.[71] This implies that the corresponding PMF has an artificial extremum at this distance. However, for distances that are short compared to this limit, it appears that periodicity-induced artifacts are rather weak[60] for small monovalent ions in solvents of high dielectric permittivity (besides the overall free-energy offset discussed previously, in the case of nonneutral systems[72]). For this reason, PMFs computed through lattice-sum methods are generally assumed to represent correctly the bulk behavior for short (compared to the unit-cell size) interionic distances.[74−78] This assumption is, however, incorrect for large ions or for charges in the neighborhood of a sizable low-dielectric cavity.[73]

The importance of lattice-sum artifacts in explicit-solvent simulations of larger (e.g., biomolecular) solutes still remains an open question. In principle, these methods represent a very good approximation for treating the electrostatic interactions in crystal simulations (although they neglect static and dynamical disorder within the crystal), and should be the method of choice.[79−81] However, for the simulation of solutions, artificial periodicity is clearly a concern. For model solutes (including a small protein) in water, a study of the dependence of the potential energy on the solute orientation within the unit cell indicated that lattice-sum rotational artifacts are small when a solvent of high permittivity is considered.[82] This conclusion was based on the assumption that solvent screening effectively results in the scaling of the direct Coulomb interactions by the solvent permittivity, which can be questioned in the case of a large solute cavity. However, this finding was confirmed by explicit-solvent simulations of a zwitterionic tetrapeptide in solution,[83] suggesting that rotational artifacts are indeed negligible in water for solutes involving a small low-dielectric cavity. In terms of possible conformational artifacts, a comparison of three 1.5 ns explicit-solvent simulations of a DNA dodecamer using the PME method and different unit-cell sizes did not evidence a significant size dependence in the monitored properties (root-mean-square deviation from the crystallographic structure and DNA curvature).[84] A similar study[85] based on 1 ns simulations of DNA oligomers also suggested little influence of the unit-cell size on the structure and dynamics. These results may indicate the absence of lattice-sum artifacts in these specific systems, but also possibly a poor convergence or weak sensitivity of the selected observables.

On the other hand, a continuum-electrostatics study of biomolecules based on simple unfolding pathways[25] suggested that artificial periodicity significantly stabilizes the most compact conformation of these molecules (i.e., generally the native state). A similar continuum-electrostatics analysis was applied to configurations of a small hyperthermophilic protein sampled during a 1 ns explicit-solvent simulation (at 550 K) employing the P^{3}M method.[25] The results showed a periodicity-induced stabilization of the folded state with respect to the most unfolded configurations observed during the simulation by about 3−4 kJ·mol^{-1} (0.7−0.9 k_BT), an effect that could help to explain the unexpected stability of the protein during the explicit-solvent simulation at 550 K.[24] In another study, the unit-cell dimensions were found to affect significantly the conformational equilibrium of a zwitterionic polyalanine octapeptide in explicit-solvent simulations using the P^{3}M method.[86] During 2 ns simulations, the peptide remained folded (α-helix) and rather rigid in a cubic box of 2 nm edge, folded but more flexible in a 3 nm box, and spontaneously unfolded in a 4 nm box. A continuum-electrostatics analysis of the configurations sampled during these simulations provided strong evidence that these effects are a consequence of artificial periodicity in the electrostatic interactions. An independent continuum-electrostatics investigation of the same peptide in the α-helical configuration reached conclusions in good qualitative agreement with these findings.[49]

The investigation of periodicity-induced artifacts in membrane systems (e.g., lipid bilayers) is also of importance. Because membrane systems involve a large low-dielectric cavity, are inherently less well solvated compared to other types of biomolecular systems, and are strongly anisotropic, these artifacts are expected to be significant. The impact of switching from a conventional cutoff-truncation scheme (after 6 ns) to Ewald summation (during 7 ns) in the course of the simulation of a 2 × 28 and a 2 × 56 L-α-dimyristoylphosphatidylcholine (DMPC) bilayer was investigated.[87] The change from a cutoff-based to a lattice-sum method resulted in a reduction of the lateral diffusion of the DMPC molecules and in a contraction of the computational box along the membrane plane. This observation was rationalized by the sudden inclusion of additional charge pairs (all periodic copies of the charges) into the electrostatic interactions, leading to a strong coupling in the motions of individual molecules, and an increase in the surface tension of the bilayer. A similar observation had been reported earlier based on shorter simulations.[88] In contrast to these findings, a recent paper[89] discussing simulations of several bundles of the ion-channel peptide alamethicin immersed in a palmitoyloleolylphosphatidylcholine (POPC) bilayer considers the use of the PME method superior to that of a straight cutoff or of the reaction-field method.[29]

The presence or absence of lattice-sum artifacts in biomolecular simulations is likely to be influenced by the ionic strength. Intuitively, it is expected that the inclusion of counterions represents an additional source of electrostatic screening within the periodic system, and thereby reduces the magnitude of periodicity-induced artifacts. In the absence of explicit counterions, lattice-sum methods implicitly neutralize the computational box containing a charged biomolecule by the inclusion of a homogeneous background charge density. Such a charge distribution, however, is a poor model for a counterion

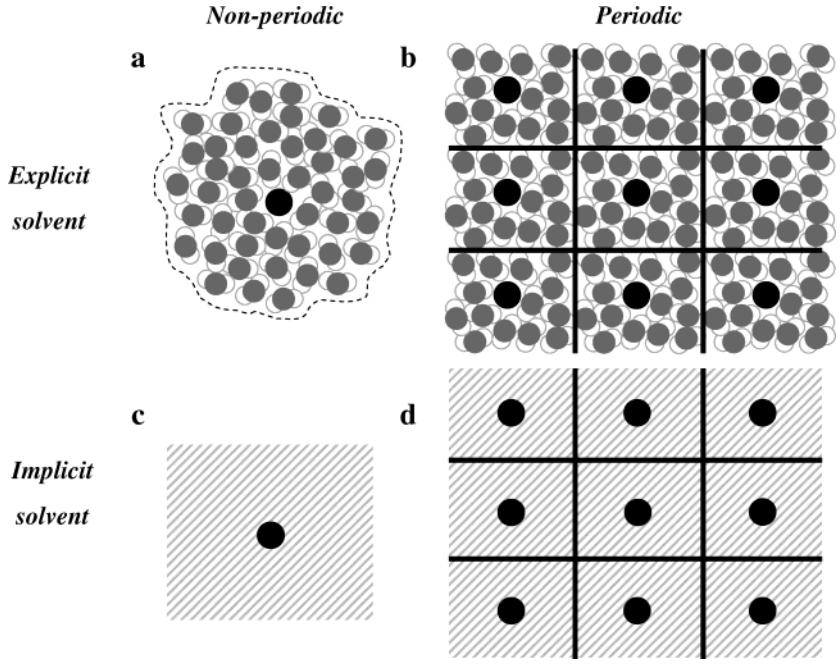

Figure 1. Nonperiodic and periodic boundary conditions as applied to explicit- and implicit-solvent calculations. The solute is symbolized by a black sphere and the solvent by water molecules (explicit solvent) or a shaded area (implicit solvent). An accurate explicit-solvent simulation under nonperiodic boundary conditions (a) would require a very large system to eliminate finite-size and surface effects, and is thus computationally intractable. For this reason, explicit-solvent simulations are commonly carried out under periodic boundary conditions (b). The corresponding perturbation can be investigated by comparing, for individual solute configurations, the results of implicit-solvent calculations under nonperiodic (c) and periodic (d) boundary conditions, leading to an estimate of the periodicity-induced perturbation of the electrostatic free energy $\Delta\Delta G_{el}$.

atmosphere, in particular because it does not depend on the local time-dependent electrostatic potential generated by the biomolecule and overlaps with the solute cavity. On the other hand, the explicit inclusion of counterions raises the problem of the slow equilibration of ionic coordinates (possibly inducing a dependence of the simulated properties on their initial placement) and of the perturbation they may induce on the system dynamics (a disruptive effect due to the small size and high charge density of the ions).

Two recent studies investigate the effect of ionic strength on the stability of proteins when lattice-sum methods are used.[90−92] The first study[90,91] discusses 1 ns simulations of the WW domain (37-residue protein, net charge $-2e$) using the PME method either with or without a neutralizing amount of counterions. Interestingly, the protein is only stable in the presence of explicit counterions, while the simulations omitting counterions result in a breakdown of the protein secondary structure. The second study[92] reports simulations of the βARK1 PH domain GRK2 (119 residues, net charge $+6e$) using the PME method either with a compensating amount (0.56 ns) or with an excess (4 ns) of counterions. It is found that the presence of counterions has a significant impact on the simulated properties, presumably related to their electrostatic screening ability. The problem of the equilibration of the counterion distribution is also discussed. It is suggested that two factors enhancing the relaxation of the explicit counterion atmosphere are an initial placement of the ions at a sufficiently large distance from the protein surface and the inclusion of an excess of counterions, both leading to faster diffusion of the ions within the system.

The aim of the present study is to further the understanding of periodicity and ionic-strength effects in lattice-sum simulations of charged biomolecules. To this purpose, a series of explicit-solvent molecular dynamics (MD) simulations of two charged biomolecules (a small protein and an oligonucleotide) employing the P^{3}M method are analyzed. The simulations of the two systems are systematically performed with zero, a minimal (neutralizing) set of, or an excess amount of counterions. In addition, to further examine the effect of artificial periodicity and ionic strength on conformational equilibria, all simulations are carried out either close to room temperature or at an artificially-elevated temperature of 500 K intended to promote the denaturation of the biomolecule.

Configurations sampled during the explicit-solvent MD simulations are analyzed using continuum electrostatics to estimate the periodicity-induced perturbation of the electrostatic free energy ($\Delta\Delta G_{el}$) along the trajectories.[8,25,60,86] This quantity corresponds to the difference in the electrostatic free energy of the system upon going from (ideal) nonperiodic boundary conditions (NPBC) to PBC, and thus provides a quantitative estimate of the amount of artificial (de)stabilization of specific configurations caused by enforcing exact periodicity of the electrostatic interactions during the simulation.

Theory

PBC are commonly used in explicit-solvent simulations because it is computationally intractable to simulate a (bio)-molecule in a solvent droplet (NPBC) of such dimensions that finite-size and surface effects become negligible, and the bulk solvation behavior is accurately reproduced (part a vs part b of Figure 1). Although this simple trick eliminates surface effects (the surface of an infinite periodic system is located at an infinite distance from the reference solute molecule), the use of PBCs in combination with a small computational box may still give rise to strong finite-size effects. This is because artificial periodicity introduces spurious interactions between the reference solute molecule and its own periodic copies, as well as a perturbation of the solvation due to the interaction of the solvent molecules with the periodic copies of the solute.[60] These effects would be largely reduced[93] by the application of cutoff truncation (possibly with a reaction-field correction) to the electrostatic interactions. Unfortunately, truncation methods

with the small cutoff radii typically used in simulations introduce other (cutoff-related) artifacts, which have an even more dramatic effect on the simulated properties. In contrast, lattice-sum algorithms take full account of periodicity in the electrostatic interactions, and periodicity-induced finite-size effects are a serious concern here.

Because the simulation of a quasi-macroscopic solvent droplet (NPBC) is computationally intractable (Figure 1a), the direct assessment of periodicity-induced artifacts in explicit-solvent simulations is not possible. At best, indirect hints toward the presence or absence of such artifacts can be obtained by varying the box size in simulations under PBC.[84−86] However, this direct comparison may be performed if an implicit-solvent model is used under either NPBC or PBC (part c vs part d of Figure 1), as an approximation to the explicit-solvent behavior. Assuming that the periodicity-induced perturbation of the nonpolar interactions (usually short-ranged) is negligible compared to the perturbation of the electrostatic interactions, the key quantity for the characterization of lattice-sum artifacts is the periodicity-induced perturbation of the electrostatic free energy ($\Delta\Delta G_{el}$). This quantity is defined, for a given solute configuration, as the difference between the total electrostatic free energy of the system upon going from NPBC to PBC, as estimated using the implicit-solvent model (part c vs part d of Figure 1). This free-energy change has two contributions:[60] (i) the periodicity-induced perturbation of the Coulomb energy (ΔE_{Cb}) arising from the interaction between the reference solute molecule and its own periodic copies (and with a homogeneous neutralizing background charge density in the case of nonneutral systems) and (ii) the periodicity-induced perturbation of the solvation free energy ($\Delta\Delta G_{solv}$) arising from the interaction of the solvent molecules with the periodic copies of the solute, so that

$$\Delta\Delta G_{el} = \Delta E_{Cb} + \Delta\Delta G_{solv} \quad (1)$$

The details of the computation of these two terms based on continuum electrostatics, involving the numerical solution of the Poisson equation for a medium of heterogeneous dielectric permittivity, have been described previously in detail and will not be repeated here.[60] The key assumption underlying this continuum-electrostatics analysis is that the observations made using an implicit-solvent model are (at least qualitatively) relevant for assessing the nature and magnitude of periodicity-induced artifacts in explicit-solvent simulations.

Computational Details

A. Systems and Setup. To investigate periodicity-induced artifacts, two biomolecular test systems were selected: a small protein and an oligonucleotide. The protein is the insulin gene enhancer protein ISL-1 (entry 1BW5[94,95] of the Protein Data Bank), a 66-residue protein with a net charge of $+11e$ that binds DNA in vivo. The initial solute configuration was generated from a set of 50 NMR structures (determined at $T = 282$ K), by averaging the coordinates and performing an energy minimization. The protein was immersed in a rectangular box of dimensions $5.63 \times 5.96 \times 7.05$ nm^3 filled with 7532 SPC[96] water molecules, resulting in a minimal solute-to-wall distance of 1.2 nm. The oligonucleotide is the double-stranded DNA dodecamer d(CGCATATATGCG)$_2$ with a net charge of $-22e$. The initial coordinates were taken from a crystallographic structure (entry 1DN9[97] of the Protein Data Bank). This oligonucleotide has been previously simulated under low-salt conditions[98] using the AMBER force field[99] and shown to undergo a reversible transition between the B and A forms within a 2 ns simulation. The dodecamer was immersed in a cubic box of dimensions $6.58 \times 6.53 \times 6.56$ nm^3 filled with 9192 SPC[96] water molecules, resulting in a minimal solute-to-wall distance of 1 nm. Six MD simulations were carried out for each of the two systems, corresponding to three amounts of counterions (zero, minimal set, or excess) and two different temperatures (low and high). The minimal set of counterions was just sufficient to neutralize the system (protein, 11 Cl^- ions; oligonucleotide, 22 Na^+ ions). The excess amount corresponded to 3 times this minimal set (protein, 22 Cl^- ions + 11 Na^+ ions; oligonucleotide, 44 Na^+ ions + 22 Cl^- ions). The lower temperature was close to room temperature (protein, 282 K; oligonucleotide, 300 K), and the higher temperature was set far above the boiling point of water (protein and oligonucleotide, 500 K), to drive the unfolding of the biomolecule on the nanosecond time scale. The initial counterion coordinates were determined by successively replacing water molecules with the lowest (Na^+) or highest (Cl^-) electrostatic potential by an ion, while preserving a minimal interionic distance of 0.35 nm. Both systems were slowly heated over a time of 100 ps to reach the lower system temperature (protein, 282 K; oligonucleotide, 300 K) using positional restraints of decreasing magnitude. This was followed by an equilibration period (protein, 300 ps; oligonucleotide, 100 ps) at constant temperature (lower temperature) and pressure (1 bar). The configurations at the end of this equilibration period were taken as initial configurations for the production runs at both low and high temperatures, which were carried out at constant volume for 1.6 ns (protein) and 1.8 ns (oligonucleotide). The high-temperature simulations of the protein were later extended to a total duration of 3 ns.

The temperature and pressure (equilibration only) were both maintained using a weak-coupling scheme,[100] with coupling constants $\tau_T = 0.1$ ps (temperature; solute and solvent coupled separately) and $\tau_P = 0.5$ ps (pressure). The equations of motion were integrated using the leapfrog algorithm with a time step of 2 fs. Bond lengths were constrained by application of the SHAKE procedure[101] with a relative geometric tolerance of 10^{-4}. All simulations were performed with the GROMOS 43a1 force field[102,103] and the SPC[96] water model, using a modified version of the GROMOS96 program[104] implementing the P^{3}M method[3,8] for calculating the electrostatic interactions. The latter method relied on a spherical hat charge-shaping function[105] of radius 0.75 nm, a charge-assignment function of order 3, a finite-difference operator of order 2, $70 \times 70 \times 70$ grid points to span the computational box, tinfoil boundary conditions, and the use of two alias vectors for the calculation of the optimal influence function. Real-space electrostatic interactions as well as van der Waals interactions were truncated at a cutoff distance of 1.0 nm on the basis of a charge-group pairlist updated every five simulation steps.

A summary of the systems and simulation conditions corresponding to the 12 simulations is given in Table 1, together with the codes used in the present article to refer to them.

B. Analysis. The periodicity-induced perturbation of the electrostatic free energy ($\Delta\Delta G_{el}$) was evaluated on the basis of continuum electrostatics as described previously[60] for 3200 (protein) or 3600 (oligonucleotide) solute configurations sampled at 0.5 ps intervals during the 12 explicit-solvent simulations excluding the 0.4 ns (protein) or 0.2 ns (oligonucleotide) equilibration time. For simulations including counterions, the ions were treated as part of the solute. In this case, the choice of a solute configuration under NPBC is somewhat arbitrary. In the present study, the choice was made to gather the

TABLE 1: Summary of the Simulated Systems and Simulation Conditions

simulation[a]	solute	ions	water	box edges (nm)[b]	T (K)	I[c] (m)
P0L, P0H	ISL-1		7532	5.66, 6.00, 7.10	L, 282; H, 500	0.45 (0.00)
P1L, P1H	ISL-1	11 Cl^-	7521	5.66, 6.00, 7.10	L, 282; H, 500	0.49 (0.04)
P2L, P2H	ISL-1	11 Na^+, 22 Cl^-	7499	5.66, 6.00, 7.10	L, 282; H, 500	0.57 (0.12)
D0L, D0H	DNA		9192	6.62, 6.62, 6.62	L, 300; H, 500	1.46 (0.00)
D1L, D1H	DNA	22 Na^+	9170	6.62, 6.62, 6.62	L, 300; H, 500	1.53 (0.07)
D2L, D2H	DNA	44 Na^+, 22 Cl^-	9126	6.62, 6.62, 6.62	L, 300; H, 500	1.67 (0.20)

[a] Codes used in the article to refer to specific simulations (P and D denote the protein and oligonucleotide simulations; 0, 1, and 2 indicate zero, a minimal set of, and an excess of counterions; L and H indicate low and high temperature). [b] Values after the constant-pressure equilibration period. [c] Ionic strength (total and, between parentheses, counterions only).

counterions by periodicity around the center of geometry of the biomolecule.

The solvation contribution $\Delta\Delta G_{solv}$ to $\Delta\Delta G_{el}$ (eq 1) represents the difference in the solvation free energy of the reference solute molecule upon going from NPBC to PBC. For each solute configuration, the latter quantity was computed by solving the Poisson equation under PBC using box dimensions identical to those used in the corresponding explicit-solvent MD run. The former quantity was computed by solving the Poisson equation under NPBC. In this case, the box-edge lengths were increased by 2 nm with respect to the unit-cell dimensions used in the MD simulation, to increase the distances between the solute atoms and the surface of the computational volume. The potential $\phi_b(\vec{r})$ at the surface of this enlarged volume was then approximated as the Coulomb potential generated by the set of N solute atomic charges q_i at locations $\vec{r}_i$ in a homogeneous medium with permittivity ϵ_s equal to that of the solvent, i.e.

$$\phi_b(\vec{r}) = \sum_{i=1}^{N} \frac{q_i}{4\pi\epsilon_0\epsilon_s||\vec{r} - \vec{r}_i||} \tag{2}$$

where ϵ_0 is the permittivity of a vacuum. Under both NPBC and PBC, the solution of the Poisson equation was obtained through a finite-difference algorithm using a modified version of the UHBD program.[106] For compatibility with the MD simulations, the atomic charges and radii were derived from the GROMOS96 force field,[102] the latter defined as $R = (2C_{12}/C_6)^{1/6}$, where C_6 and C_{12} are the parameters defining the Lennard-Jones interaction of a given atom with an SPC water oxygen. The dielectric boundary was defined as the contact and reentrant surface obtained by rolling a probe of 0.14 nm radius over the solute. The solute and solvent permittivities were set to $\epsilon_i = 1$ (vacuum) and $\epsilon_s = 78$ (water), respectively, and the grid spacing was set to 0.1 nm. The sensitivity of the results on the specific choice of grid spacing and computational volume (NPBC only) was tested to ensure that changes in these parameters did not alter the calculated free energies significantly (data not shown).

The Coulomb contribution ΔE_{Cb} to $\Delta\Delta G_{el}$ (eq 1) represents the difference between the electrostatic energy of the solute alone in a medium of homogeneous permittivity ϵ_i upon going from NPBC to PBC. For each solute configuration, the latter quantity was computed by applying the P^{3}M method using box dimensions identical to those used in the corresponding explicit-solvent MD run, but omitting the solvent molecules. The former quantity was computed by summing pairwise Coulomb interactions within the solute molecule (no periodicity, no cutoff truncation). The Wigner self-term (arising from the interaction of charges with their own periodic copies and the homogeneous neutralizing background charge density) was included in the electrostatic energy under PBC whenever required (nonneutral systems). The solute permittivity was set to $\epsilon_i = 1$ for these calculations.

In addition to the properties mentioned above, several other quantities were calculated from the MD trajectories. The root-mean-square backbone atomic positional deviation from the native structure (RMSD), the number of hydrogen bonds (HB), the secondary structure content, the radius of gyration (R_{gyr}), the solute-only square dipole moments (μ_s, $\tilde{\mu}_s$), and the solute−counterion square dipole moments (μ_t and $\tilde{\mu}_t$) were monitored as a function of time. The RMSD was calculated as the deviation of the backbone atoms (protein, atom types CA, N, and C; oligonucleotide, atom types C4*, C5*, O5*, P, O3*, and C3*) with respect to the energy-minimized average NMR (protein) or crystallographic (oligonucleotide) structure. The HB were calculated by defining the presence of a hydrogen bond D−H···A through a H···A distance smaller than 0.25 nm and a D−H···A angle larger than 135°. The secondary structure content was attributed according to the secondary-structure definition of Kabsch and Sander[107] and calculated using the program PROCHECK.[108] The square dipole moments μ_s, $\tilde{\mu}_s$, μ_t, and $\tilde{\mu}_t$ were calculated as

$$\mu = -\sum_{i}\sum_{j>i} q_i q_j \vec{r}_{ij}^{\,2} \tag{3}$$

where the summation runs over all atom pairs (excluding ions for μ_s and $\tilde{\mu}_s$, or including them for μ_t and $\tilde{\mu}_t$) and $\vec{r}_{ij}$ is the minimum-image vector (for μ_s and μ_t) or the connecting vector (for $\tilde{\mu}_s$ and $\tilde{\mu}_t$) in the system gathered by periodicity around the solute center of geometry. The quantity μ is equal to the square of the dipole moment for a neutral system and represents a generalized definition otherwise. In addition, for the protein, the polar surface area (POL), the apolar surface area (APOL), the end-to-end distance (DIST), and the wing-to-wing (WDIST) distance were monitored as a function of time. The quantities POL and APOL were calculated using the program NACCESS.[109] The distance WDIST was defined as the distance between the center of geometry for the backbone atoms of the first and last six amino acid residues. This quantity was defined because the N- and C-terminal residues of the protein form flexible and highly charged wings as opposed to the rigid three-helix core, and might therefore strongly interact with their periodic copies in the course of the simulations. The root-mean-square atomic positional fluctuations (RMSF) were calculated for all backbone atoms on the basis of the interval 0.4−2.0 ns (protein) or 0.2−2.0 ns (oligonucleotide). The translational diffusion coefficients (D) for the ions were calculated from the corresponding mean-square displacements via the Einstein relation

$$D = \lim_{t\to\infty} \frac{1}{6t}[\langle|\vec{r}_i(t) - \vec{r}_i(0)|^2\rangle] \tag{4}$$

where $\vec{r}_i(t)$ is the coordinate of the ion at time t within the infinite periodic system (i.e., including lattice translations due to the crossing of box boundaries).

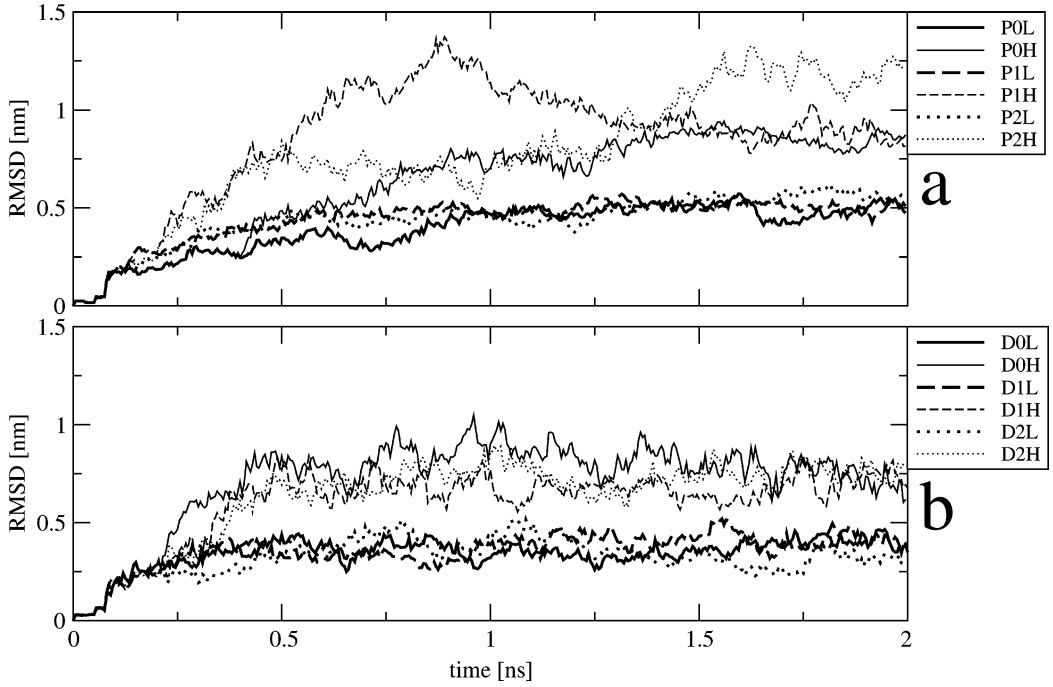

Figure 2. Time series of the RMSD with respect to the energy-minimized average NMR (protein) or crystallographic (oligonucleotide) structures, for the protein (a) and oligonucleotide (b) simulations. The curves include a 0.4 ns (protein) or 0.2 ns (oligonucleotide) equilibration time. Simulation codes refer to Table 1.

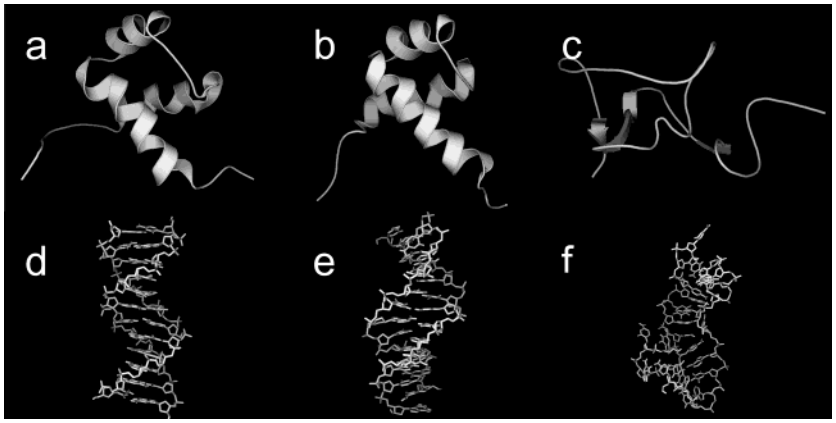

Figure 3. Schematic representation of the starting structures (a, d) and of the final structures of the P1L (b), P1H (c), D1L (e), and D1H (f) simulations.

For the protein simulations, positive violations with respect to the 827 experimental NOE-derived distance upper bounds were calculated along the trajectories using an $\langle r^{-6}\rangle^{-1/6}$ distance averaging over the interval 0.4−2.0 ns, and the pseudoatom corrections derived by Fletcher et al.[110]

Results

The discussion of the results refers to the nomenclature and simulation conditions reported in Table 1.

A. Structural Properties. The time series of the RMSD of the solute coordinates with respect to the energy-minimized average NMR (protein) or crystallographic (oligonucleotide) structures are displayed in parts a and b of Figure 2 for the protein and oligonucleotide simulations, respectively. For both systems, the low-temperature simulations involving different amounts of counterions do not exhibit significant differences in terms of RMSD values. These converge to about 0.45 nm after 1 ns (protein) and about 0.35−0.4 nm after 0.5 ns (oligonucleotide), and remain approximately constant thereafter. For the high-temperature protein simulations, the two systems including counterions (P1H, P2H) tend to have larger RMSD values and fluctuations compared to the simulation without counterions (P0H). On the basis of the RMSD alone, one may therefore argue that the absence of counterions leads to a somewhat reduced overall structural deviation from the native structure at elevated temperature. For the oligonucleotide high-temperature simulations, no similar observation can be made. In these three simulations, the RMSD fluctuates around a common value of 0.7 nm reached after about 0.5 ns. In terms of structural rearrangements, the low-temperature protein and oligonucleotide simulations essentially preserve the initial structure, as shown for the simulations with a minimal set of counterions in parts b and e, respectively, of Figure 3. In contrast, the high-temperature simulations lead to a denaturation of the initial structures (Figure 3c,f).

For the protein simulations, the positive violations with respect to NOE-derived distance upper bounds[94] are additional quantities indicating how well the simulation compares with experimentally-derived structural information. The maximum and average violations corresponding to the six protein simula-

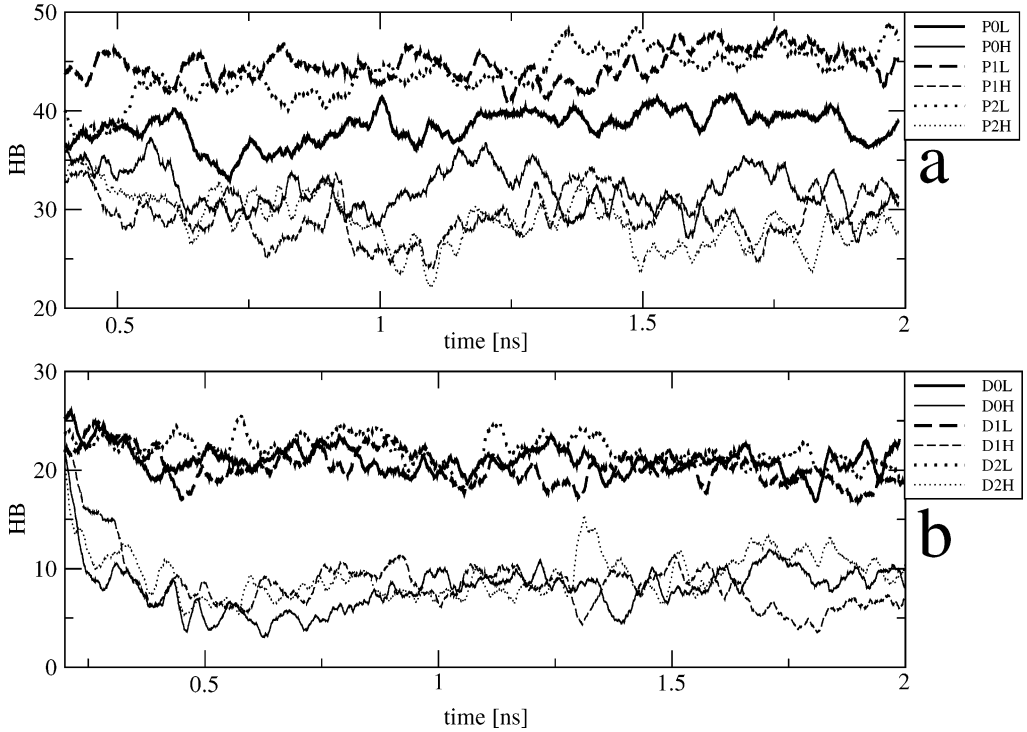

Figure 4. Time evolution of the HB for the protein (a) and oligonucleotide (b) simulations. The curves exclude a 0.4 ns (protein) or 0.2 ns (oligonucleotide) equilibration time. The native structures of the two biomolecules contain 24 (protein) and 33 (oligonucleotide) hydrogen bonds. Simulation codes refer to Table 1.

TABLE 2: Maximum and Average Positive Violations with Respect to the 827 Experimental NOE-Derived Distance Upper Bounds[94] [a]

simulation	max violation (nm)	av violation (nm)
NMR	0.001	0.001
P0L	0.154	0.001
P0H	0.379	0.009
P1L	0.252	0.002
P1H	0.177	0.002
P2L	0.149	0.001
P2H	0.107	0.002

[a] Results are given for the six protein simulations based on $\langle r^{-6}\rangle^{-1/6}$ averaging over the interval 0.4−2.0 ns. Simulation codes refer to Table 1. Data corresponding to the set of 50 NMR structures[94] are reported for comparison (label NMR).

tions are reported in Table 2. The average violations are very low for all simulations (<0.01 nm in all cases). This result is somewhat surprising considering the magnitude of the RMSD values for the high-temperature simulations, and is an indication that rather diverse structural ensembles may satisfy the experimentally-determined NOE upper bounds equally well. Finally, it appears that the simulation P0H has the highest maximal and average violations, which is somewhat at odds with the preceding considerations on the basis of RMSD values (Figure 2a).

The time series of HB are displayed in parts a and b of Figure 4 for the protein and oligonucleotide simulations, respectively. For the low-temperature protein simulations the number of hydrogen bonds is systematically lower (by about 5) in the simulation without counterions (P0L). No similar observation can be made for the low-temperature oligonucleotide simulations, where the numbers of hydrogen bonds are nearly identical, irrespective of the amount of counterions included. Note that the number of hydrogen bonds in the low-temperature protein simulations is larger than the corresponding number in the native structure (24), while the opposite is true for the oligonucleotide, where the simulation shows a lower number of hydrogen bonds compared to the native structure (33). This observation probably reflects intrinsic differences in the behavior of the GROMOS96 force fields for proteins and nucleic acids, and in the quality of the two experimentally-determined structures. For the high-temperature protein simulations, hydrogen bonds are slightly more numerous in simulation P0H. However, this trend is not found in the corresponding high-temperature oligonucleotide simulations, which are all very similar.

The RMSD (Figure 2a) and HB (Figure 4a) analyses (but not the NOE violations, Table 2) suggest a somewhat increased stability of the protein native structure at high temperature in simulation P0H. A similar observation can be made from the evolution of the secondary structure content as a function of time, displayed in Figure 5. While both simulations P1H and P2H show a rapid (within 1−1.5 ns) melting of the three helices (residues 12−25, 30−40, and 42−58), the corresponding simulation without counterions retains a significant amount of secondary structure for a longer time, and the first helix until the end of the simulation. Whether this slightly increased stability of the native structure at elevated temperature in the absence of counterions is related to the unscreened interaction between the protein and its periodic images, or to a possible disruptive effect of the counterions remains unclear. At low temperature, the three protein simulations preserve the secondary structure content essentially intact throughout the simulations (Figure 3).

The backbone RMSF for the protein and oligonucleotide simulations are displayed in parts a and b, respectively, of Figure 6. This observable provides a measure of the structural mobility within the solute molecule, and is important here because it has been suspected that the artificial periodicity enforced by lattice-sum methods tends to reduce the conformational fluctuations of biomolecules.[21,112] As expected, the high-temperature simulations show larger fluctuations compared to the low-

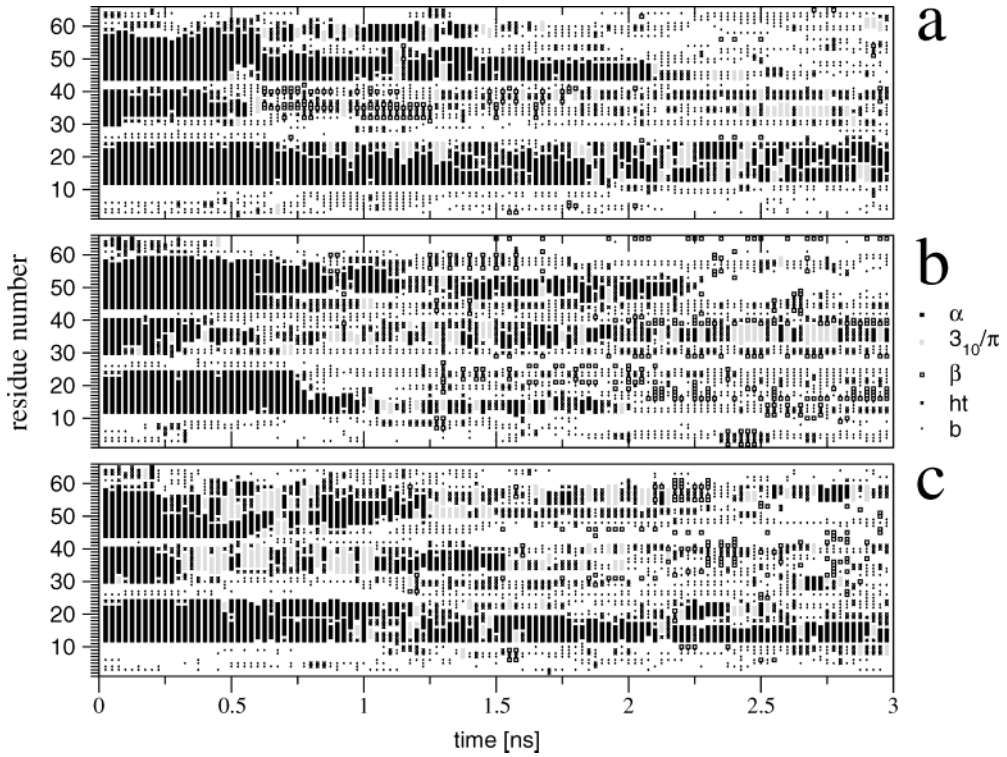

Figure 5. Time evolution of the secondary structure content for the protein simulations at high temperature. The three graphs correspond to simulations with zero (a; P0H), a minimal set of (b; P1H), or an excess amount of (c; P2H) counterions. These results correspond to simulations extended to a total duration of 3 ns (including a 0.4 ns equilibration time). The symbols refer to the following secondary structure elements: α-helix (α); 3_{10}- or π-helix ($3_{10}/\pi$); β-sheet (β); hydrogen-bonded turn (ht); bend (b).

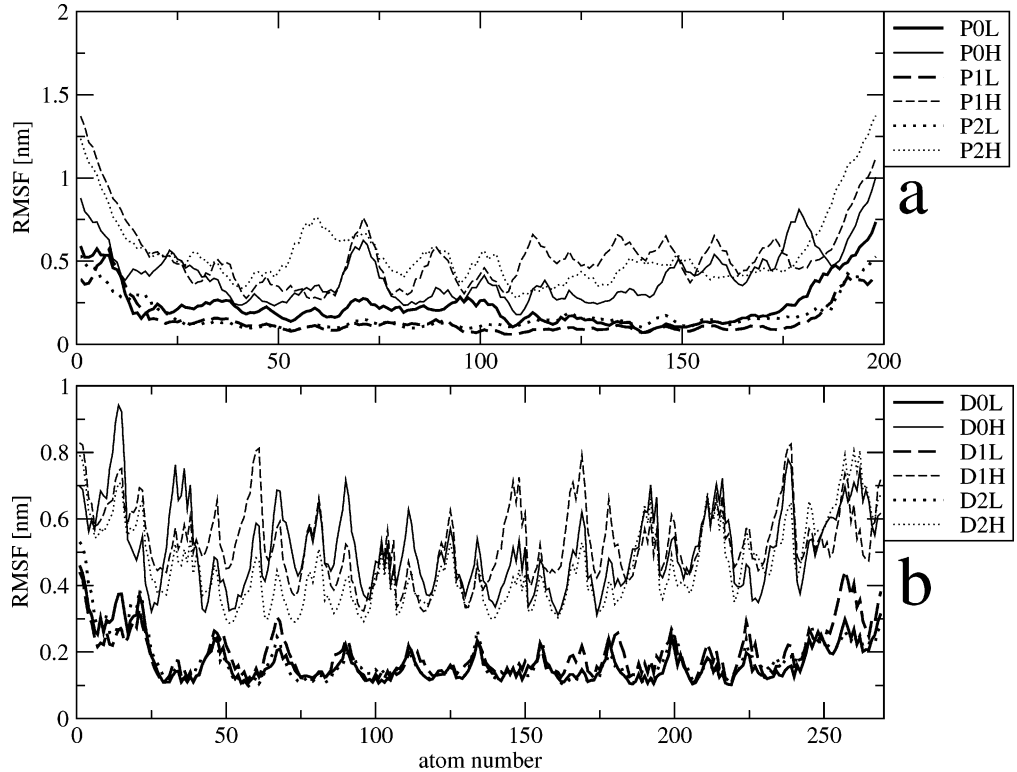

Figure 6. RMSF of the protein backbone atoms (a) and of all oligonucleotide atoms (b), displayed as a function of the atom number. For the oligonucleotide, the average RMSF for both strands is plotted. The locations of the RMSF maxima coincide with the phosphate groups. Simulation codes refer to Table 1.

temperature ones. At low temperature, the only significant difference between the RMSF values is the slightly higher fluctuations in simulation P0L. This observation is consistent with the slightly lower number of hydrogen bonds observed during this simulation (Figure 4a). For the high-temperature protein simulations, the average RMSF (P0H, 0.41 nm; P1H, 0.52 nm; P2H, 0.54 nm) are somewhat larger for the simulations including counterions. For the oligonucleotide the corresponding averages (D0H, 0.51 nm; D1H, 0.53 nm; D2H, 0.46 nm) do not show a similar trend.

TABLE 3: Diffusion Coefficient of the Counterions[a]

simulation	Na^+ (10^{-5} cm^2 s^{-1})	Cl^- (10^{-5} cm^2 s^{-1})
P1L		1.4
P1H		9.7
P2L	1.9	1.2
P2H	6.6	7.9
D1L	1.7	
D1H	8.2	
D2L	1.6	2.5
D2H	9.4	8.1

[a] Simulation codes refer to Table 1.

Since a limited ionic mobility can in principle lead to structural distortions in the solvated biomolecule when explicit counterions are included, it is of interest to calculate the translational diffusion coefficient for the different ionic species. The corresponding values are reported in Table 3. The low-temperature diffusion coefficients for Na^+ [$(1.6-1.9) \times 10^{-5}$ cm^2 s^{-1}] and Cl^- [$(1.2-2.5) \times 10^{-5}$ cm^2 s^{-1}] are in good agreement with experimental values (Na^+, 1.33×10^{-5} cm^2 s^{-1}; Cl^-, 2.03×10^{-5} cm^2 s^{-1}) for the diffusion of these ions in pure water at 300 K.[113] As expected, the diffusion coefficients increase with increasing temperature. However, they show only moderate variations with increasing counterion concentration. The trend is rather toward a slight decrease in ionic mobility with increasing ionic strength (in contrast with a previous suggestion[92]), which may result from the favorable interaction between ions of opposite charges. Overall, this analysis indicates that both the limited box sizes and the high net charges of the biomolecules considered do not affect ionic diffusion significantly. This is illustrated in Figure 7, where a representative trajectory of two ions in the P2L simulation is displayed over a time interval of 0.4 ns. The other counterions also diffuse freely in the computational box on the nanosecond time scale, without remaining locked at their initial position. Indeed, on the basis of a diffusion constant of 1.5×10^{-5} cm^2 s^{-1}, an ion is expected to travel a mean distance of 3×10^5 nm (i.e., about half the box edge length) within 1 ns.

B. Periodicity-Induced Perturbation of the Electrostatic Free Energy. The time evolution of the periodicity-induced perturbation $\Delta\Delta G_{el}$ of the electrostatic free energy, and of its components ΔE_{Cb} and $\Delta\Delta G_{solv}$, is displayed for the low-temperature protein simulations without (P0L) or with a minimal set (P1L) of counterions in parts a and b, respectively, of Figure 8. In both cases, the quantities ΔE_{Cb} and $\Delta\Delta G_{solv}$ are of similar magnitudes but opposite signs, while their time evolutions are almost perfectly anticorrelated. The corresponding correlation coefficients are -0.997 (P0L) and -0.999 (P1L). This indicates that the direct Coulomb interaction between the reference solute molecule (possibly including the neighboring counterions) is very efficiently screened by the solvent, as a consequence of its high dielectric permittivity. A similar anticorrelation has been observed previously.[25,60] Note that ΔE_{Cb} and $\Delta\Delta G_{solv}$ are about 1 order of magnitude larger in the case of a nonneutral system (P0L) compared to a neutral one (P1L). Due to the strong anticorrelation between direct Coulomb and solvation effects, the fluctuations in the sum $\Delta\Delta G_{el}$ of the two components are much smaller in magnitude than the fluctuations in either of the two components. The root-mean-square fluctuations in $\Delta\Delta G_{el}$ amount to only 2.46 kJ·mol^{-1} (P0L) or 1.1 kJ·mol^{-1} (P1L). Note also that the discontinuities in the time evolution of ΔE_{Cb} and $\Delta\Delta G_{solv}$ for the P1L simulation, which are due to the diffusion of the counterions across the boundary of the reference unit cell, largely cancel out in $\Delta\Delta G_{el}$. Because the solvent screening (although efficient) is only partial, the fluctuations in the overall periodicity-induced perturbation of the electrostatic free energy $\Delta\Delta G_{el}$ keep a significant degree of correlation with their Coulomb component ΔE_{Cb}. The corresponding correlation coefficients are 0.54 (P0L) and 0.95 (P1L), while the slopes are about 1/22 (P0L) and 1/74 (P1L). A high correlation coefficient between $\Delta\Delta G_{el}$ and ΔE_{Cb} and a slope close to ϵ_s^{-1} are to be expected for the simulations including counterions. This is because, in this case, the periodicity-induced effect is dominated by the (small and spherical) counterions, for which $\Delta\Delta G_{solv} \approx (\epsilon_s^{-1} - 1)\Delta E_{Cb}$.[60] The solvent screening is less efficient for large solute molecules such as a protein, resulting in a poorer correlation and a slope larger than ϵ_s^{-1} for the simulation without counterions. The corresponding correlation coefficients, intercepts, and slopes are reported in Table 4 for all simulations. The results confirm the above suggestion. For the neutral systems, the slopes range from 1/71 to 1/82 (very close to ϵ_s^{-1}), while the intercepts are small. In this case, using $\Delta\Delta G_{el} \approx \epsilon_s^{-1}\Delta E_{Cb}$, as done in a previous investigation of lattice-sum artifacts,[82] is a meaningful approximation. However, for the nonneutral systems, the calculated slopes range from 1/22 to 1/55, while the intercepts may be very large. In this case, the above approximation is certainly not valid and the conclusions of this type of analysis[82,83] are questionable. Finally, in the absence of counterions, one observes a negative offset of about -55 kJ·mol^{-1} in $\Delta\Delta G_{el}$. This offset, which is only present for simulations involving a nonneutral unit cell, is essentially due to the interaction of the solute charges with their own periodic copies and the neutralizing background charge density filling the unit cell. It is analogous to the offset observed in the solvation free energy of a single spherical ion under PBC.[60] For a reasonably small (compared to the unit-cell size) spherical ion of charge q, this offset amounts to

$$\Delta\Delta G_{el}^{ion} \approx -2.837297\frac{q^2}{8\pi\epsilon_0\epsilon_s L} \qquad (5)$$

Inserting the protein charge of $+11e$, the solvent permittivity

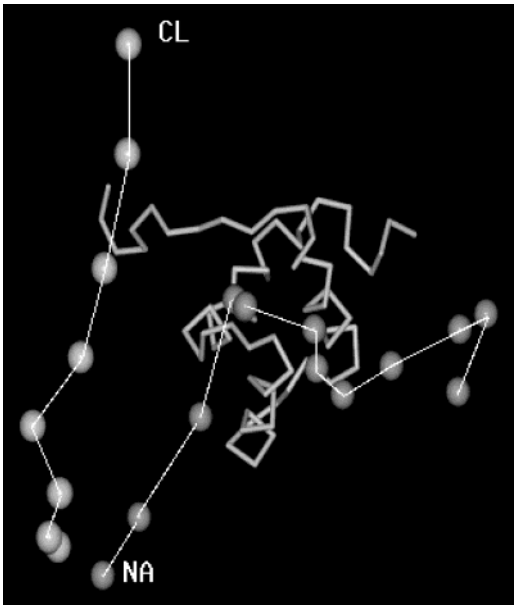

Figure 7. Representative trajectories of two counterions (one Na^+ and one Cl^-) over a time period of 0.44 ns during the low-temperature protein simulation with an excess of counterions (P2L). The backbone trace of the native protein structure is shown as a reference.

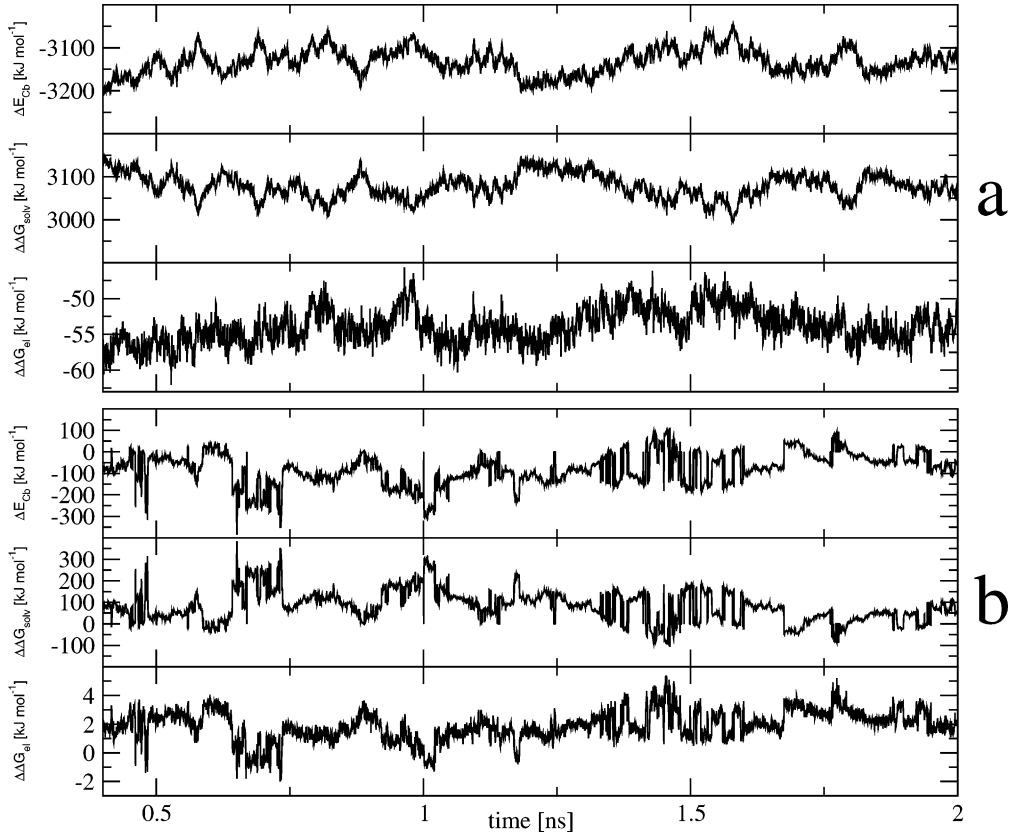

Figure 8. Time evolution of the periodicity-induced perturbation $\Delta\Delta G_{el}$ of the electrostatic free energy, and of its components ΔE_{Cb} and $\Delta\Delta G_{solv}$, for the low-temperature protein simulations without (a; P0L) or with a minimal set (b; P1L) of counterions.

TABLE 4: Slope, Intercept, and Linear Correlation Coefficient Corresponding to the Periodicity-Induced Perturbation of the Electrostatic Free Energy $\Delta\Delta G_{el}$ as a Function of the Periodicity-Induced Perturbation of the Coulomb Energy ΔE_{Cb}[a]

simulation	slope	intercept (kJ·mol^{-1})	correlation coeff (kJ·mol^{-1})
P0L	1/22	89.1	0.54
P0H	1/55	2.2	0.38
P1L	1/74	3.0	0.95
P1H	1/82	2.7	0.86
P2L	1/71	4.9	0.98
P2H	1/76	4.9	0.97
D0L	1/42	67.7	0.66
D0H	1/55	−1.5	0.29
D1L	1/76	1.5	0.90
D1H	1/81	1.9	0.94
D2H	1/79	6.0	0.95
D2L	1/80	5.8	0.95

[a] Simulation codes refer to Table 1.

of 78, and $L \approx 6.25$ nm gives a $\Delta\Delta G_{el}^{ion}$ of −49 kJ·mol^{-1}, in good qualitative agreement with the present value of −55 kJ·mol^{-1}.

The time evolutions of the periodicity-induced perturbation of the electrostatic free energy $\Delta\Delta G_{el}$ for the protein and oligonucleotide simulations are displayed in parts a and b, respectively, of Figure 9. This time evolution can be analyzed in terms of three main properties: the average value, drift along the simulations, and magnitude of the fluctuations. These quantities are summarized in Table 5.

The simulations without counterions are characterized by a large negative average value of $\Delta\Delta G_{el}$, while the average values for simulations including counterions are very close to zero. As mentioned previously, a negative offset is expected for the simulation of a nonneutral unit cell, and essentially arises from the interaction of the solute charges with their own periodic copies and the homogeneous neutralizing background charge density filling the unit cell.[60] This offset is roughly 4 times larger for the oligonucleotide compared to the protein, in agreement with the fact that the solute overall charge is 2 times larger. However, this global offset in $\Delta\Delta G_{el}$ is of no significance in the present study. This is because it affects equally all configurations sampled during the simulation, and thus cannot influence the dynamics of the system.

The drifts in $\Delta\Delta G_{el}$, expressed on a per-nanosecond basis, are smaller than 1 k_BT (2.5 or 4.2 kJ·mol^{-1} at 300 or 500 K) in magnitude for all simulations. This suggests that periodicity-induced artifacts do not drive by themselves any major conformational change on the nanosecond time scale. However, these drifts remain nonnegligible for some simulations. Positive values larger than 1 kJ·mol^{-1}·ns^{-1} in magnitude are observed for simulations P0L, P2L, and D0L. Negative values larger than 1 kJ·mol^{-1}·ns^{-1} in magnitude are observed for simulations P0H, D0H, and D2L. In simulation D0H, the magnitude of the drift (−3.53 kJ·mol^{-1}·ns^{-1}, i.e., 0.85 k_BT at 500 K) is large enough to suggest that artificial periodicity may contribute as a nonnegligible driving force to the unfolding pathway selected by the oligonucleotide.

Finally, in the absence of a major drift, the fluctuations of $\Delta\Delta G_{el}$ provide an indication about the amount of periodicity-induced (de)stabilization of specific configurations with respect to the others. For both the protein and oligonucleotide systems, these fluctuations are smallest (1.0−1.4 kJ·mol^{-1}, about 0.5 k_BT at 300 K) in the systems including a minimal set of counterions. The simulations excluding counterions or including an excess of counterions show fluctuations of $\Delta\Delta G_{el}$ that are roughly 2−3 times larger in magnitude. The range of the variations in $\Delta\Delta G_{el}$

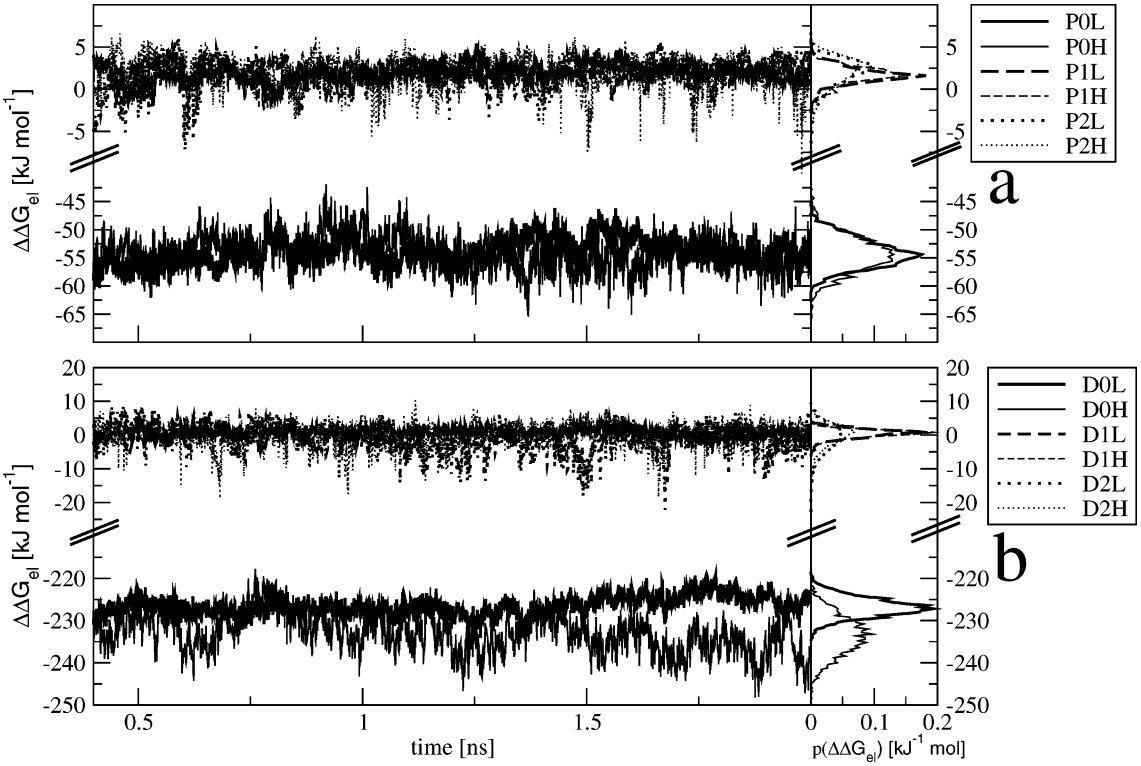

Figure 9. Time evolution of the periodicity-induced perturbation of the electrostatic free energy $\Delta\Delta G_{el}$, together with its distribution $p(\Delta\Delta G_{el})$, for the protein (a) and the oligonucleotide (b) simulations. Simulation codes refer to Table 1.

TABLE 5: Parameters Characterizing the Time Evolution of the Periodicity-Induced Perturbation of the Electrostatic Free Energy $\Delta\Delta G_{el}$[a]

simulation	average (kJ·mol^{-1})	drift (kJ·mol^{-1}·ns^{-1})	fluctuation (kJ·mol^{-1})	range (kJ·mol^{-1})
P0L	−53.92	1.66	2.46	16.35
P0H	−54.13	−1.35	3.16	23.54
P1L	1.85	0.71	1.01	3.40
P1H	1.77	−0.17	1.09	3.03
P2L	1.42	1.18	2.62	7.30
P2H	2.03	−0.55	2.03	5.00
D0L	−226.64	1.82	2.29	14.93
D0H	−233.12	−3.53	4.46	29.08
D1L	0.75	−0.13	1.39	0.60
D1H	0.25	0.53	1.38	1.30
D2L	−0.75	−1.55	3.81	5.00
D2H	−0.32	0.22	3.71	8.50

[a] The average values, drifts (slope from a linear regression), root-mean-square fluctuations, and ranges (maximal minus minimal value) of $\Delta\Delta G_{el}$ are based on the time interval 0.4−2.0 ns (protein) or 0.2−2.0 ns (oligonucleotide). Simulation codes refer to Table 1. See also Figure 9.

(maximal minus minimal value) provides an indication about the maximal amount of periodicity-induced (de)stabilization between any two sampled configurations. This quantity is again smallest in the simulations with a minimal set of counterions (0.6−3.4 kJ·mol^{-1}), larger in simulations with an excess of counterions (5.0−8.5 kJ·mol^{-1}), and very large for the simulations without counterions (14.9−29.1 kJ·mol^{-1}, about an order of magnitude larger than 1 k_BT). Recalling that the population bias resulting from a perturbation $\Delta\Delta G$ of the free energy is proportional $e^{-\Delta\Delta G/(k_BT)}$, this periodicity-induced perturbation is clearly significant in the context of explicit-solvent molecular dynamics simulations. From this point of view, the present results suggest that the inclusion of a minimal (neutralizing) set of counterions in explicit-solvent simulations of charged biomolecules is to be preferred over any other choice, limiting the $\Delta\Delta G_{el}$ fluctuations and range of variation to about 0.5 and 1 k_BT, respectively. The observed increase in $\Delta\Delta G_{el}$ fluctuations upon going from a minimal set to an excess amount of counterions may tentatively be explained by an increased probability of creating a sizeable instantaneous dipole moment in the reference unit cell (by motion of the counterions), which correlates with equivalent dipole moments in the neighboring unit cells. The larger fluctuation of $\Delta\Delta G_{el}$ in the absence of counterions is probably due to the larger magnitudes of the ΔE_{Cb} and $\Delta\Delta G_{solv}$ contributions and of the corresponding fluctuations, together with the poorer anticorrelation between these quantities. In other words, a counterion atmosphere, whenever present, can adjust to the fluctuations of the electrostatic potential created by the solute charges, and efficiently screen the interaction between the solute and its periodic images. In contrast, a fixed homogeneous neutralizing background charge cannot adjust to these fluctuations.

C. Structural Effect of Artificial Periodicity. The above analysis of the time evolution of $\Delta\Delta G_{el}$ reveals that specific configurations are significantly (de)stabilized by artificial periodicity. The obvious next step is to investigate whether $\Delta\Delta G_{el}$ is correlated with structural or energetical properties of the system. For example, in a previous study of a zwitterionic polyalanine octapeptide[86] $\Delta\Delta G_{el}$ showed a strong negative correlation with the end-to-end distance of the peptide, which allowed for a structural interpretation of the observed artifacts. In the present case, correlations of $\Delta\Delta G_{el}$ (and its contributions ΔE_{Cb} and $\Delta\Delta G_{solv}$) with a number of structural and energetical properties were systematically investigated. The results of this analysis are reported in Tables 6 and 7 for the protein and oligonucleotide simulations, respectively.

Besides the previously-discussed correlations of ΔE_{Cb} with $\Delta\Delta G_{solv}$ (−0.99 in all cases), $\Delta\Delta G_{el}$ with ΔE_{Cb} ($\geq$0.85 for all simulations including counterions) and $\Delta\Delta G_{el}$ with $\Delta\Delta G_{solv}$ ($\leq$−0.85 for all simulations including counterions), the observed

TABLE 6: Correlation between the Periodicity-Induced Perturbation of the Electrostatic Free Energy $\Delta\Delta G_{el}$ (or Its Two Components ΔE_{Cb} and $\Delta\Delta G_{solv}$) and Structural or Energetical Properties of the System for the Protein Simulation[a]

	$\Delta\Delta G_{el}$						ΔE_{Cb}						$\Delta\Delta G_{solv}$					
	P0L	P0H	P1L	P1H	P2L	P2H	P0L	P0H	P1L	P1H	P2L	P2H	P0L	P0H	P1L	P1H	P2L	P2H
ΔE_C[c]	0.54	0.38	0.95	0.86	0.98	0.97	1.00	1.00	1.00	1.00	1.00	1.00	−0.99	−0.99	−0.99	−0.99	−0.99	−0.99
$\Delta\Delta G_{solv}$	−0.48	−0.34	−0.95	−0.85	−0.98	−0.97	−0.99	−0.99	−0.99	−0.99	−0.99	−0.99	1.00	1.00	1.00	1.00	1.00	1.00
μ_s[b]	0.61	0.41	0.01	−0.19	−0.07	−0.08	0.68	0.67	−0.02	−0.22	−0.05	−0.06	−0.66	−0.66	0.03	0.22	0.05	0.06
$\tilde{\mu}_s$[b]	0.63	0.44	0.04	−0.17	−0.09	−0.08	0.89	0.89	0.0	−0.08	−0.07	−0.07	−0.88	−0.88	0.0	0.08	0.07	0.07
μ_t[b]			0.34	−0.11	0.64	0.03			0.29	−0.16	0.60	0.03			−0.29	0.16	−0.60	−0.03
$\tilde{\mu}_t$[b]			0.06	0.18	0.69	0.27			0.01	0.10	0.65	0.26			−0.01	−0.10	−0.65	−0.26
RMSD[c]	0.42	−0.13	0.12	−0.09	0.53	−0.09	0.22	0.30	0.08	0.00	0.50	−0.06	−0.18	−0.31	−0.08	0.00	−0.50	0.06
R_{gyr}[d]	0.36	0.28	−0.01	−0.13	−0.20	−0.12	0.48	0.31	−0.08	−0.11	−0.19	−0.11	−0.47	−0.30	0.08	0.11	0.19	0.11
DIST[e]	0.44	0.31	−0.19	−0.03	0.18	−0.10	0.45	0.32	−0.23	−0.04	0.16	−0.09	−0.43	−0.31	0.23	0.04	−0.16	0.09
WDIST[f]	0.08	−0.25	0.11	0.01	0.00	−0.08	0.23	−0.58	0.17	−0.12	0.02	−0.05	−0.23	0.57	−0.17	0.13	−0.02	0.05
POL[g]	0.16	0.04	0.03	0.06	−0.53	−0.09	0.28	0.02	−0.00	−0.01	−0.49	−0.09	−0.28	−0.02	0.00	0.01	0.49	0.09
APOL[h]	−0.19	0.28	−0.21	0.05	−0.56	0.01	−0.05	0.02	−0.23	−0.04	−0.51	−0.03	0.04	0.00	0.23	0.04	0.51	0.03
HB[i]	0.06	0.00	−0.02	−0.01	0.23	0.02	−0.04	−0.06	−0.00	−0.01	0.22	0.03	0.04	0.06	0.00	0.01	−0.22	−0.03

[a] Correlation coefficients for the given property as a function of $\Delta\Delta G_{el}$, ΔE_{Cb}, or $\Delta\Delta G_{solv}$ are reported from a linear regression analysis over the interval 0.4−2.0 ns. Simulation codes refer to Table 1. [b] Square solute dipole moment based on four alternative definitions (see eq 3 and related discussion). [c] Root-mean-square backbone atomic positional deviation. [d] Radius of gyration. [e] End-to-end distance. [f] Distance between protein "wings" at the N and C termini. [g] Polar solvent-exposed surface area. [h] Apolar solvent-exposed surface area. [i] Total number of hydrogen bonds.

TABLE 7: Correlation between the Periodicity-Induced Perturbation of the Electrostatic Free Energy $\Delta\Delta G_{el}$ (or Its Components ΔE_{Cb} and $\Delta\Delta G_{solv}$) and Structural or Energetical Properties of the System for the Oligonucleotide Simulation[a]

	$\Delta\Delta G_{el}$						ΔE_{Cb}						$\Delta\Delta G_{solv}$					
	D0L	D0H	D1L	D1H	D2L	D2H	D0L	D0H	D1L	D1H	D2L	D2H	D0L	D0H	D1L	D1H	D2L	D2H
ΔE_{Cb}	0.66	0.29	0.90	0.94	0.95	0.95	1.00	1.00	1.00	1.00	1.00	1.00	−0.99	−0.99	−0.99	−0.99	−0.99	−0.99
$\Delta\Delta G_{solv}$	−0.64	−0.22	−0.90	−0.94	−0.95	−0.95	−0.99	−0.99	−0.99	−0.99	−0.99	−0.99	1.00	1.00	1.00	1.00	1.00	1.00
μ_s[b]	0.69	0.20	−0.01	0.02	−0.15	−0.03	0.86	0.31	−0.09	−0.02	−0.12	−0.07	−0.86	−0.31	0.10	0.02	0.12	0.07
$\tilde{\mu}_s$[b]	0.70	0.26	0.01	−0.10	−0.18	−0.04	0.95	0.62	−0.08	−0.15	−0.16	−0.07	−0.94	−0.61	0.08	0.15	0.16	0.07
μ_t[b]			0.25	−0.01	0.07	−0.03			0.04	−0.07	0.14	−0.03			−0.04	0.07	−0.14	0.03
$\tilde{\mu}_t$[b]			0.32	0.10	0.17	−0.02			0.13	0.07	0.25	0.0			−0.12	−0.07	−0.25	0.0
RMSD[c]	0.39	−0.05	0.29	0.11	0.07	−0.04	0.41	0.22	0.16	0.05	0.12	−0.06	−0.41	−0.23	−0.16	−0.04	−0.12	0.06
R_{gyr}[d]	0.35	0.0 5	−0.23	−0.05	−0.0 6	−0.07	0.66	0.42	−0.16	−0.12	−0.08	−0.13	−0.67	−0.43	0.16	0.12	0.08	0.13
HB[e]	−0.01	−0.04	0.03	−0.10	−0.02	0.01	−0.13	−0.21	0.05	−0.06	−0.02	0.02	0.14	0.21	−0.05	0.06	0.02	−0.02

[a] Correlation coefficients for the given property as a function of $\Delta\Delta G_{el}$, ΔE_{Cb}, or $\Delta\Delta G_{solv}$ are reported from a linear regression analysis over the interval 0.2−2 ns. Simulation codes refer to Table 1. [b] Square solute dipole moment based on four alternative definitions (see eq 3 and related discussion). [c] Root-mean-square backbone atomic positional deviation. [d] Radius of gyration. [e] Total number of hydrogen bonds.

correlations are typically rather low. An exception is the positive correlation of ΔE_{Cb} with μ_s (or $\tilde{\mu}_s$) in the absence of counterions. The correlation between $\Delta\Delta G_{el}$ and the RMSD is positive for all low-temperature simulations, and especially high (about 0.3−0.5) for the protein in the absence or in the presence of an excess of counterions, and for the oligonucleotide in the absence or in the presence of a minimal set of counterions. The observation of a systematic positive correlation indicates that artificial periodicity tends to stabilize the native conformation of both biomolecules at low temperature. For the high-temperature simulations, this correlation is small in magnitude (≤0.13**)** and generally negative (except for simulation D1H). Thus, under unfolding conditions, artificial periodicity may very weakly drive the system away from the native structure. The correlation of $\Delta\Delta G_{el}$ with R_{gyr} and DIST (protein only) is positive and significant (about 0.3−0.4) for the simulations without counterions (except simulation D0H). Thus, in this case, the sampling also appears to be biased toward compact configurations. The correlation with POL and APOL (protein only) shows no clear trend, besides a strong negative correlation for simulation P2L. Finally, the correlation with HB is systematically very low in magnitude (≤0.23), indicating that artificial periodicity has very little influence on the number of intramolecular hydrogen bonds.

D. Correcting Structural Observables for the Effect of Artificial Periodicity. The fact that the periodicity-induced perturbation of the electrostatic free energy $\Delta\Delta G_{el}$ is available from the continuum-electrostatics analysis for successive solute configurations suggests a possible way to correct simulated observables for the effect of artificial periodicity. Within the limit of a weak periodicity-induced perturbation, this correction can be performed using the one-step perturbation formula,[114] as

$$X_c = \frac{\langle x(t) e^{\beta\Delta\Delta G_{el}(t)} \rangle}{\langle e^{\beta\Delta\Delta G_{el}(t)} \rangle} \tag{6}$$

where $x(t)$ is an instantaneous observable leading to the (uncorrected) simulation average $X_u = \langle x(t) \rangle$ and $\beta = (k_B T)^{-1}$. The uncorrected and corrected averages corresponding to several structural properties of the system are reported in Table 8. In general, the differences between uncorrected and corrected RMSD values are rather small (between −0.01 and +0.01 nm) except for simulations P0L (+0.03), D0L (+0.04 nm), and D0H (−0.03 nm). In most cases, the correction leads to a slight increase in the RMSD value for the low-temperature simulations and a slight decrease for the high-temperature ones. This is consistent with the results of the correlation analysis (Tables 6 and 7), suggesting that artificial periodicity stabilizes the native conformation in the low-temperature simulations, and destabilizes it in the high-temperature regime. The differences between uncorrected and corrected RMSF values is also small (between −0.02 and +0.02) and tends to be negative (except for simulations D0H and D1H). Thus, unexpectedly, artificial periodicity tends to slightly increase the solute fluctuations, especially in the low-temperature simulations. As expected from

TABLE 8: Application of the Perturbation Formula To Correct Simulated Observables for the Effect of Artificial Periodicity[a]

simulation	$(\mathrm{RMSD})_u$ (nm)	$(\mathrm{RMSD})_c$ (nm)	$(\mathrm{RMSF})_u$ (nm)	$(\mathrm{RMSF})_c$ (nm)	$(R_{gyr})_u$ (nm)	$(R_{gyr})_c$ (nm)	$(\mathrm{HB})_u$	$(\mathrm{HB})_c$	$(\mathrm{SHB})_u$	$(\mathrm{SHB})_c$	$(\mu_s)_u$ (e·nm)	$(\mu_s)_c$ (e·nm)	$(\mu_t)_u$ (e·nm)	$(\mu_t)_c$ (e·nm)
P0L	0.44	0.47	0.27	0.25	1.38	1.39	36.4	38.8	162.9	162.5	280.2	300.9		
P0H	0.73	0.72	0.48	0.47	1.25	1.27	32.0	31.7	124.2	124.7	269.4	279.0		
P1L	0.49	0.49	0.18	0.18	1.30	1.30	44.7	44.6	150.3	150.1	194.4	194.5	−711.0	−706.5
P1H	0.99	0.98	0.58	0.58	1.56	1.55	29.3	29.3	124.8	125.1	362.1	360.2	−650.1	−653.7
P2L	0.49	0.50	0.18	0.18	1.40	1.40	43.8	44.2	148.3	149.2	242.3	243.8	−467.7	−456.6
P2H	0.90	0.89	0.62	0.62	1.49	1.49	28.8	28.9	126.2	126.2	343.1	341.0	−504.5	−507.5
D0L	0.44	0.48	0.19	0.18	2.43	2.40	21.1	20.9			869.9	898.3		
D0H	0.92	0.89	0.54	0.56	2.82	2.92	8.2	8.2			976.1	994.9		
D1L	0.49	0.50	0.15	0.14	2.81	2.88	20.1	20.2			−3342.8	−3362.8	871.1	872.5
D1H	0.86	0.86	0.56	0.57	2.01	1.93	8.3	8.1			−3084.2	−3086 .1	873.3	873.9
D2L	0.44	0.45	0.19	0.18	1.59	1.45	21.9	22.4			−2615.6	−2650.8	800.2	793.0
D2H	0.78	0.78	0.51	0.51	3.11	3.11	9.9	9.9			−2648.7	−2632.9	839.8	839.5

[a] The observables considered are the root-mean-square backbone atomic positional deviation (RMSD), the average root-mean-square backbone atomic positional fluctuations (RMSF), the radius of gyration (R_{gyr}), the total number of solute−solute hydrogen bonds (HB), the total number of solute−solvent hydrogen bonds (SHB), and the square dipole moment based on four alternative definitions (see eq 3 and related discussion). The uncorrected averages computed directly from the simulation (u subscript) and the corresponding corrected values (c subscript) calculated via the perturbation formula (eq 6) are reported. The averages are performed over the interval 0.4−2.0 ns (protein) or 0.2−2.0 ns (oligonucleotide). Simulation codes refer to Table 1.

the correlation analysis (Tables 6 and 7), the correction by application of the perturbation formula has little effect on the average number of intrasolute hydrogen bonds. Similarly, the number of solute−solvent hydrogen bonds is essentially unaffected. Note, however, that increasing the ionic strength tends to decrease the number of hydrogen bonds to the solvent in the low-temperature simulations, especially upon going from a neutralizing amount to an excess of counterions. No similar trend is seen in the high-temperature simulations.

Conclusion

The aim of the present study was to examine the nature and magnitude of periodicity-induced artifacts arising from the use of lattice-sum algorithms in simulations of charged biomolecules at different ionic strengths and temperatures.

The analysis of several time-resolved structural properties along the 12 independent simulations did not reveal striking or systematic differences between the systems involving different amounts of counterions. The most relevant observations are (i) a lower number of intrasolute hydrogen bonds and slightly larger structural fluctuations in the low-temperature protein simulation without counterions and (ii) a slightly lower deviation from the native structure and better secondary structure preservation in the high-temperature protein simulation without counterions.

Configurations sampled along the trajectories were analyzed using continuum electrostatics to evaluate the periodicity-induced perturbation of the electrostatic free energy $\Delta\Delta G_{el}$, and its Coulomb and solvation contributions ΔE_{Cb} and $\Delta\Delta G_{solv}$, respectively. The two contributions are very large in magnitude, but highly anticorrelated, resulting in an overall electrostatic perturbation $\Delta\Delta G_{el}$ of much smaller magnitude. This perturbation remains largely correlated with its Coulomb component, but is 1−2 orders of magnitude smaller. The correlation is especially strong for systems including counterions, where the ratio of ΔE_{Cb} to $\Delta\Delta G_{el}$ is approximately equal to the permittivity of the solvent. Besides a systematic (and dynamically irrelevant) offset for nonneutral systems, the absence of a systematic drift in $\Delta\Delta G_{el}$ indicates that artificial periodicity does not drive a major conformational change on the nanosecond time scale (except possibly for the high-temperature oligonucleotide simulation without counterions). However, the fluctuations in $\Delta\Delta G_{el}$ are on the order of 1 k_BT, which is significant in the context of molecular dynamics simulation; i.e., periodicity effects noticeably (de)stabilize specific configurations along the simulations. The smallest $\Delta\Delta G_{el}$ fluctuations were found with the use of a minimal (neutralizing) amount of counterions, suggesting that this choice should be the preferred one when lattice-sum simulations of charged biomolecules are set up.

It was not possible to unambiguously correlate the periodicity-induced perturbation of the electrostatic free energy with a simple structural parameter characterizing the solute conformation. It is therefore difficult to relate the energetically non-negligible bias introduced by artificial periodicity to a specific structural bias. However, for the limited set of structural observables considered in the present study, the perturbation formula could be used to correct the simulated values for the effect of artificial periodicity. The major conclusions of this analysis are that at room temperature (i) artificial periodicity tends to slightly stabilize the native configuration of the studied biomolecules (especially in the absence of counterions) without significantly affecting the magnitude of their structural fluctuations and (ii) the structural perturbation, as probed by the observables monitored here, remains extremely limited in magnitude for the solutes, solvent, and unit-cell sizes considered in the present study.

In summary, it appears that, although artificial periodicity induces a nonnegligible energetical bias (and thus affects the sampling of solute configurations), this bias results in no major structural perturbation for the systems considered here. This does not, however, exclude the possibility of a significant effect of artificial periodicity on other structural observables (e.g., counterion distributions or side chain conformations) or the presence of more dramatic periodicity-induced artifacts in other (bio)molecular systems.

Acknowledgment. The Swiss National Science Foundation (Project 2100-061939) is gratefully acknowledged for financial support.

References and Notes

(1) Madelung, E. *Phys. Z.* **1918**, *19*, 524.
(2) Ewald, P. P. *Ann. Phys. (Leipzig)* **1921**, *64*, 253.
(3) Hockney, R. W.; Eastwood, J. W. *Computer simulation using particles*; McGraw-Hill: New York, 1981.
(4) Darden, T.; York, D.; Pedersen, L. *J. Chem. Phys.* **1993**, *98*, 10089.
(5) Essmann, U.; Perera, L.; Berkowitz, M. L.; Darden, T.; Lee, H.; Pedersen, L. G. *J. Chem. Phys.* **1995**, *103*, 8577.

(6) de Leeuw, S. W.; Perram, J. W.; Smith, E. R. *Proc. R. Soc. London, Ser. A* **1980**, *373*, 27.
(7) de Leeuw, S. W.; Perram, J. W.; Smith, E. R. *Proc. R. Soc. London, Ser. A* **1980**, *373*, 57.
(8) Hünenberger, P. H. *Simulation and Theory of Electrostatic Interactions in Solution*; AIP: Melville, NY, 1999.
(9) Luty, B. A.; Davis, M. E.; Tironi, I. G.; van Gunsteren, W. F. *Mol. Simul.* **1994**, *14*, 11.
(10) Luty, B. A.; Tironi, I. G.; van Gunsteren, W. F. *J. Chem. Phys.* **1995**, *103*, 3014.
(11) Pollock, E. L.; Glosli, J. *Comput. Phys. Commun.* **1996**, *95*, 93.
(12) Deserno, M.; Holm, C. *J. Chem. Phys.* **1998**, *109*, 7678.
(13) Deserno, M.; Holm, C. *J. Chem. Phys.* **1998**, *109*, 7694.
(14) Smith, P. E.; Pettitt, B. M. *J. Chem. Phys.* **1991**, *95*, 8430.
(15) Cheatham, T. E.; Miller, J. L.; Fox, T.; Darden, T. A.; Kollman, P. A. *J. Am. Chem. Soc.* **1995**, *117*, 4193.
(16) Fox, T.; Kollman, P. A. *Proteins: Struct., Funct., Genet.* **1996**, *25*, 315.
(17) Cheatham, T. E.; Young, M. A. *Biopolymers* **2000**, *56*, 232.
(18) Cheatham, T. E.; Kollman, P. A. *Annu. Rev. Phys. Chem.* **2000**, *51*, 435.
(19) Auffinger, P.; Westhof, E. *Curr. Opin. Struct. Biol.* **1998**, *8*, 227.
(20) Allen, M. P.; Tildesley, D. J. *Computer Simulations of Liquids*; Clarendon Press: Oxford, 1987.
(21) Brooks, C. L. *Curr. Opin. Struct. Biol.* **1995**, *5*, 211.
(22) LouiseMay, S.; Auffinger, P.; Westhof, E. *Curr. Opin. Struct. Biol.* **1996**, *6*, 289.
(23) Auffinger, P.; LouiseMay, S.; Westhof, E. *J. Am. Chem. Soc.* **1996**, *118*, 1181.
(24) de Bakker, P. I. W.; Hünenberger, P. H.; McCammon, J. A. *J. Mol. Biol.* **1999**, *285*, 1811.
(25) Hünenberger, P. H.; McCammon, J. A. *Biophys. Chem.* **1999**, *78*, 69.
(26) Barker, J. A.; Watts, R. O. *Mol. Phys.* **1973**, *26*, 789.
(27) Neumann, M. *Mol. Phys.* **1983**, *50*, 841.
(28) Barker, J. A. *Mol. Phys.* **1994**, *83*, 1057.
(29) Tironi, I. G.; Sperb, R.; Smith, P. E.; van Gunsteren, W. F. *J. Chem. Phys.* **1995**, *102*, 5451.
(30) Hünenberger, P. H.; van Gunsteren, W. F. *J. Chem. Phys.* **1998**, *108*, 6117.
(31) Stocker, U.; van Gunsteren, W. F. *Proteins: Struct., Funct., Genet.* **2000**, *40*, 145.
(32) Daura, X.; Haaksma, E.; van Gunsteren, W. F. *J. Comput.-Aided Mol. Des.* **2000**, *14*, 507.
(33) Nina, M.; Simonson, T. *J. Phys. Chem. B* **2002**, *106*, 3696.
(34) Neumann, M.; Steinhauser, O. *Mol. Phys.* **1980**, *39*, 437.
(35) Pollock, E. L.; Alder, B. J. *Physica A* **1980**, *102*, 1.
(36) Alder, B. J.; Pollock, E. L. *Annu. Rev. Phys. Chem.* **1981**, *32*, 311.
(37) Adams, D. J.; Adams, E. M. *Mol. Phys.* **1981**, *42*, 907.
(38) Neumann, M.; Steinhauser, O. *Chem. Phys. Lett.* **1983**, *102*, 508.
(39) Steinhauser, O. *Chem. Phys.* **1983**, *79*, 465.
(40) Neumann, M.; Steinhauser, O. *Chem. Phys. Lett.* **1984**, *106*, 563.
(41) Neumann, M.; Steinhauser, O.; Pawley, G. S. *Mol. Phys.* **1984**, *52*, 97.
(42) de Leeuw, S. W.; Perram, J. W.; Smith, E. R. *Annu. Rev. Phys. Chem.* **1986**, *37*, 245.
(43) Smith, E. R.; Wielopolski, P. A. *Mol. Phys.* **1987**, *61*, 1063.
(44) Boresch, S.; Steinhauser, O. *Ber. Bunsen-Ges.* **1997**, *101*, 1019.
(45) Boresch, S.; Steinhauser, O. *J. Chem. Phys.* **1999**, *111*, 8271.
(46) Boresch, S.; Ringhofer, S.; Hochtl, P.; Steinhauser, O. *Biophys. Chem.* **1999**, *78*, 43.
(47) Kirkwood, J. G. *J. Chem. Phys.* **1939**, *7*, 911.
(48) Boresch, S.; Steinhauser, O. *J. Chem. Phys.* **2001**, *115*, 10780.
(49) Boresch, S.; Steinhauser, O. *J. Chem. Phys.* **2001**, *115*, 10793.
(50) Kusalik, P. G. *J. Chem. Phys.* **1990**, *93*, 3520.
(51) Belhadj, M.; Alper, H. E.; Levy, R. M. *Chem. Phys. Lett.* **1991**, *179*, 13.
(52) Roberts, J. E.; Schnitker, J. *J. Phys. Chem.* **1995**, *99*, 1322.
(53) Vorobjev, Y. N.; Hermans, J. *J. Phys. Chem. B* **1999**, *103*, 10234.
(54) Sloth, P.; Sorensen, T. S. *Chem. Phys. Lett.* **1990**, *173*, 51.
(55) Hummer, G.; Pratt, L. R.; Garcia, A. E. *J. Phys. Chem.* **1996**, *100*, 1206.
(56) Figueirido, F.; DelBueno, G. S.; Levy, R. M. *J. Phys. Chem. B* **1997**, *101*, 5622.
(57) Hummer, G.; Pratt, L. R.; Garcia, A. E. *J. Chem. Phys.* **1997**, *107*, 9275.
(58) Hummer, G.; Pratt, L. R.; Garcia, A. E. *J. Phys. Chem. A* **1998**, *102*, 7885.
(59) Sakane, S.; Ashbaugh, H. S.; Wood, R. H. *J. Phys. Chem. B* **1998**, *102*, 5673.
(60) Hünenberger, P. H.; McCammon, J. A. *J. Chem. Phys.* **1999**, *110*, 1856.
(61) Bogusz, S.; Cheatham, T. E.; Brooks, B. R. *J. Chem. Phys.* **1998**, *108*, 7070.
(62) Peter, C.; van Gunsteren, W. F.; Hünenberger, P. H. *J. Chem. Phys.* **2002**, *116*, 7434.
(63) Nijboer, B. R. A.; Ruijgrok, T. W. *J. Stat. Phys.* **1988**, *53*, 361.
(64) Cichocki, B.; Felderhof, B. U.; Hinsen, K. *Phys. Rev. A* **1989**, *39*, 5350.
(65) Hummer, G.; Soumpasis, D. M. *J. Chem. Phys.* **1993**, *98*, 581.
(66) Ashbaugh, H. S.; Wood, R. H. *J. Chem. Phys.* **1997**, *106*, 8135.
(67) Hummer, G.; Pratt, L. R.; Garcia, A. E.; Berne, B. J.; Rick, S. W. *J. Phys. Chem. B* **1997**, *101*, 3017.
(68) Aqvist, J.; Hansson, T. *J. Phys. Chem. B* **1998**, *102*, 3837.
(69) Ashbaugh, H. S.; Sakane, S.; Wood, R. H. *J. Phys. Chem. B* **1998**, *102*, 3844.
(70) Babu, C. S.; Yang, P. K.; Lim, C. *J. Biol. Phys.* **2002**, *28*, 95.
(71) Valleau, J. P.; Whittington, S. G. *A Guide to Monte Carlo for Statistical Mechanics: 1. Highways*; Plenum: New York, 1977; Vols. 5 and 6.
(72) Figueirido, F.; Delbuono, G. S.; Levy, R. M. *J. Chem. Phys.* **1995**, *103*, 6133.
(73) Luty, B. A.; van Gunsteren, W. F. *J. Phys. Chem.* **1996**, *100*, 2581.
(74) Guardia, E.; Rey, R.; Padro, J. A. *J. Chem. Phys.* **1991**, *95*, 2823.
(75) Bader, J. S.; Chandler, D. *J. Phys. Chem.* **1992**, *96*, 6423.
(76) Hummer, G.; Soumpasis, D. M.; Neumann, M. *Mol. Phys.* **1994**, *81*, 1155.
(77) DelBuono, G. S.; Figueirido, F. E.; Levy, R. M. *Chem. Phys. Lett.* **1996**, *263*, 521.
(78) Rozanska, X.; Chipot, C. *J. Chem. Phys.* **2000**, *112*, 9691.
(79) York, D. M.; Darden, T. A.; Pedersen, L. G. *J. Chem. Phys.* **1993**, *99*, 8345.
(80) Walser, R.; Hünenberger, P. H.; van Gunsteren, W. F. *Proteins: Struct., Funct., Genet.* **2001**, *43*, 509.
(81) Walser, R.; Hünenberger, P. H.; van Gunsteren, W. F. *Proteins: Struct., Funct., Genet.* **2002**, *48*, 327.
(82) Smith, P. E.; Pettitt, B. M. *J. Chem. Phys.* **1996**, *105*, 4289.
(83) Smith, P. E.; Blatt, H. D.; Pettitt, B. M. *J. Phys. Chem. B* **1997**, *101*, 3886.
(84) de Souza, O. N.; Ornstein, R. L. *Biophys. J.* **1997**, *72*, 2395.
(85) Cheatham, T. E.; Kollman, P. A. *Molecular Dynamics Simulation of Nucleic Acids in solution: How sensitive are the results to small perturbations in the force field and environment?* Adenine Press: Schenectady, NY, 1998; Vol. 1.
(86) Weber, W.; Hünenberger, P. H.; McCammon, J. A. *J. Phys. Chem. B* **2000**, *104*, 3668.
(87) Takaoka, Y.; Pasenkiewicz-Gierula, M.; Miyagawa, H.; Kitamura, K.; Tamura, Y.; Kusumi, A. *Biophys. J.* **2000**, *79*, 3118.
(88) Egberts, E.; Marrink, S. J.; Berendsen, H. J. C. *Eur. Biophys. J. Biophys. Lett.* **1994**, *22*, 423.
(89) Tieleman, D. P.; Hess, B.; Sansom, M. S. P. *Biophys. J.* **2002**, *83*, 2393.
(90) Ibragimova, G. T.; Wade, R. C. *Biophys. J.* **1998**, *74*, 2906.
(91) Ibragimova, G. T.; Wade, R. C. *Biophys. J.* **1999**, *77*, 2191.
(92) Pfeiffer, S.; Fushman, D.; Cowburn, D. *Proteins: Struct., Funct., Genet.* **1999**, *35*, 206.
(93) Wood, R. H. *J. Chem. Phys.* **1995**, *103*, 6177.
(94) Ippel, J. H.; Larsson, G.; Behravan, G.; Lundqvist, M.; Lycksell, P. O.; Schleucher, J.; Zdunek, J.; Wijmenga, S. S. *J. Biomol. NMR* **1998**, *12*, 357.
(95) Ippel, H.; Larsson, G.; Behravan, G.; Zdunek, J.; Lundqvist, M.; Schleucher, J.; Lycksell, P. O.; Wijmenga, S. *J. Mol. Biol.* **1999**, *288*, 689.
(96) Berendsen, H. J. C. *Interaction Models for Water in Relation to Protein Hydration*, Intermolecular Forces ed.; Reidel: Dordrecht, The Netherlands, 1981.
(97) Yoon, C.; Prive, G. G.; Goodsell, D. S.; Dickerson, R. E. *Proc. Natl. Acad. Sci. U.S.A.* **1988**, *85*, 6332.
(98) Real, A. N.; Greenall, R. J. *J. Mol. Model.* **2000**, *6*, 654.
(99) Cornell, W. D.; Cieplak, P.; Bayly, C. I.; Gould, I. R.; Merz, K. M.; Ferguson, D. M.; Spellmeyer, D. C.; Fox, T.; Caldwell, J. W.; Kollman, P. A. *J. Am. Chem. Soc.* **1995**, *117*, 5179.
(100) Berendsen, H. J. C.; Postma, J. P. M.; van Gunsteren, W. F.; Dinola, A.; Haak, J. R. *J. Chem. Phys.* **1984**, *81*, 3684.
(101) Ryckaert, J. P.; Ciccotti, G.; Berendsen, H. J. C. *J. Comput. Phys.* **1977**, *23*, 327.
(102) van Gunsteren, W. F.; Billeter, S. R.; Eising, A. A.; Hünenberger, P. H.; Krüger, P.; Mark, A. E.; Scott, W. R. P.; Tironi, I. G. *Biomolecular Simulation: The GROMOS96 Manual and User Guide*; Verlag der Fachvereine Hochschulverlag AG an der ETH Zürich: Zürich, Switzerland, 1996.

(103) Daura, X.; Mark, A. E.; van Gunsteren, W. F. *J. Comput. Chem.* **1998**, *19*, 535.
(104) Scott, W. R. P.; Hunenberger, P. H.; Tironi, I. G.; Mark, A. E.; Billeter, S. R.; Fennen, J.; Torda, A. E.; Huber, T.; Kruger, P.; van Gunsteren, W. F. *J. Phys. Chem. A* **1999**, *103*, 3596.
(105) Hünenberger, P. H. *J. Chem. Phys.* **2000**, *113*, 10464.
(106) Madura, J. D.; Davis, M. E.; Gilson, M. K.; Wade, R. C.; Luty, B. A.; McCammon, J. A. *Biological Applications of Electrostatic Calculations and Brownian Dynamics Simulations*; VCH: New York, 1994; Vol. 4.
(107) Kabsch, W.; Sander, C. *Biopolymers* **1983**, *22*, 2577.
(108) Laskowski, R. A.; Macarthur, M. W.; Moss, D. S.; Thornton, J. M. *J. Appl. Crystallogr.* **1993**, *26*, 283.
(109) Hubbard, S. J.; Thornton, J. M. *NACCESS*, 2.0 ed.; University College London: London, 1993.
(110) Fletcher, C. M.; Jones, D. N. M.; Diamond, R.; Neuhaus, D. *J. Biomol. NMR* **1996**, *8*, 292.
(111) van Gunsteren, W. F.; Billeter, S. R.; Eising, A. A.; Hünenberger, P. H.; Krüger, P.; Mark, A. E.; Scott, W. R. P.; Tironi, I. G. *Biomolecular Simulation: The GROMOS96 Manual and User Guide*; Verlag der Fachvereine Hochschulverlag AG an der ETH Zürich: Zürich, Switzerland, 1996.
(112) Cheatham, T. E.; Kollman, P. A. *J. Mol. Biol.* **1996**, *259*, 434.
(113) Atkins, P. W. *Physical Chemistry*, 6th ed.; Oxford University Press: Oxford, 1998.
(114) Zwanzig, R. W. *J. Chem. Phys.* **1954**, *22*, 1420.